Journal of Alloys and Compounds 980 (2024) 173631

Contents lists available at ScienceDirect

Journal of Alloys and Compounds

journal homepage: www.elsevier.com/locate/jalcom

Evolution of charge density wave order in continuous solid solutions Lu($Ni_{1-x}Co_x$)C_2 ☆

Herwig Michor [a,*], Marta Roman [a,b], Lisa Reisinger [a], Maria Fritthum [a], Jana Schmelzenbart [a], Alexander Vock [a], Volodymyr Levytskyi [c], Volodymyr Babizhetskyy [d,*], Bogdan Kotur [d]

[a] Institute of Solid State Physics, TU Wien, Wiedner Hauptstrasse 8–10, A-1040 Wien, Austria
[b] Institute of Physics and Applied Computer Science, Faculty of Applied Physics and Mathematics and Advanced Materials Center, Gdansk University of Technology, Narutowicza 11 / 12, 80–233 Gdansk, Poland
[c] Institut für Experimentelle Physik, TU Bergakademie Freiberg, Leipziger Straße 23, 09596 Freiberg, Germany
[d] Department of Inorganic Chemistry, Ivan Franko National University of Lviv, Kyryla i Mefodiya Str. 6, 79005 Lviv, Ukraine

ARTICLE INFO

Keywords:
Carbometalates
$CeNiC_2$-type structure
Quasi-binary phase diagram
Charge density wave

ABSTRACT

Pseudo-ternary solid solutions, Lu($Ni_{1-x}Co_x$)C_2 ($0 \le x \le 1$), were studied by means of powder X-ray diffraction, differential thermal analysis as well as electrical resistivity and heat capacity measurements. The crystal structure of the Lu($Ni_{1-x}Co_x$)C_2 series, as investigated by means of X-ray powder diffraction, is of structure type $CeNiC_2$, space group *Amm*2, Pearson symbol *oS*8. The structural analysis reveals a non-monotonous evolution, in particular for the *a*- and *c*-lattice parameters, resulting in a non-linear decrease of the unit cell volume, markedly deviating from Vegard's rule, due to non-isoelectronic substitution of Ni by Co. Utilizing differential thermal analysis (DTA) data, a pseudo-binary phase diagram $LuNiC_2$–$LuCoC_2$ has been constructed. The evolution of charge density wave order in Lu($Ni_{1-x}Co_x$)C_2, which reaches an ordering temperature $T_{CDW} \cong 450$ K for $LuNiC_2$, was studied by means of electrical resistivity and heat capacity measurements. For solid solutions prepared via the floating-zone melting technique it became feasible to trace charge density wave (CDW) features of the temperature dependent electrical resistivity, thus, indicating a critical composition for the suppression of CDW order in Lu($Ni_{1-x}Co_x$)C_2 at around $x \approx 0.15 - 0.17$, which matches with a distinct drop of the composition dependent electronic Sommerfeld coefficient of the low temperature heat capacity of Ni-rich solid solutions.

1. Introduction

Ternary rare-earth nickel dicarbides $RNiC_2$ (R = Y, La→Lu) crystallize in the $CeNiC_2$ structure type: orthorhombic space group *Amm*2 [1,2], whereas $RCoC_2$ compounds (R = rare-earth) display two structure types: the $CeCoC_2$-type structure with the monoclinic space group *Cc* for R being a light rare-earth metal [2], and the $CeNiC_2$-type structure for R being a heavy rare-earth. Both structure types are representatives of carbometalates, where closely bound C–C dimers are a characteristic structure building elements [3]. Recently, carbometalates $RNiC_2$ became of particular interest as, except for $LaNiC_2$ and $CeNiC_2$, they all undergo charge density wave (CDW) transitions and many of them (R = Ce, Nd, Gd→Tm) display low-temperature antiferromagnetism, while $SmNiC_2$ orders ferromagnetically at $T_C = 17.7$ K [4–11].

Discontinuous solid solutions in the pseudo-binary system Ce($Ni_{1-x}Co_x$)C_2 were studied in our earlier work [12]. The orthorhombic $CeNiC_2$-type structure preserves in the alloys with $0 \le x \le 0.2$, while the $CeCoC_2$-type structure is stable in the Ni/Co composition range $0.5 \le x \le 1$. The non-isoelectronic substitution of Ni by Co in the solid solution Ce($Ni_{1-x}Co_x$)C_2 causes a continuous reduction of the Néel temperature, and, for $CeCoC_2$, results in a paramagnetic Kondo-lattice ground state with a characteristic Kondo temperature, $T_K \approx 30$ K [12].

Continuous solid solutions with $CeNiC_2$-type structure occur in the following $RNiC_2$-$RCoC_2$ pseudo-binary systems: R = Tb, Dy, Ho [13–16]. The substitution of Ni by Co changes the number of conduction electrons and influences the strength of the magnetic exchange interactions between the rare-earth moments. The crystal structure and magnetic properties of solid solutions R($Ni_{1-x}Co_x$)C_2 (R = Tb, Dy, Ho) were reported to display a non-monotonous crossover from ferromagnetic to antiferromagnetic ground states [13,15,16]. In the Dy($Ni_{1-x}Co_x$)C_2 and

☆ In memory of Professor Vitaly Pecharsky

* Corresponding authors.
E-mail addresses: michor@ifp.tuwien.ac.at (H. Michor), volodymyr.babizhetskyy@lnu.edu.ua (V. Babizhetskyy).

https://doi.org/10.1016/j.jallcom.2024.173631
Received 31 October 2023; Received in revised form 15 January 2024; Accepted 21 January 2024
Available online 23 January 2024

$Ho(Ni_{1-x}Co_x)C_2$ systems, Ni/Co substitution causes a remarkable deviation of the unit cell volume from Vegard's rule and a non-monotonous variation of the *a* and *c* lattice parameters. A crossover from ferromagnetic to antiferromagnetic ordering is accompanied with a significant reduction of the magnetic ordering temperature [15,16].

An important aspect of the isostructural ($CeNiC_2$ structure type) quasi-ternary systems $R(Ni_{1-x}Co_x)C_2$ with R = Gd → Lu, which has not yet been revealed experimentally, is the expected existence of a critical point (critical Ni/Co composition) of the CDW phase, because the $RCoC_2$ (R = Gd – Lu) compounds do not show any CDW features and CDW order has been explicitly ruled out for $LuCoC_2$ [8]. Composition or pressure induced critical points of CDW order are of particular interest as there are observations of superconducting domes at around critical points of CDW order. A prominent example of enhanced superconductivity next to a CDW quantum critical point is $Lu(Pt_{1-x}Pd_x)_2In$ [17]. In the case of $LaNiC_2$, which shows highly unconventional superconductivity but no CDW order at ambient pressure [18–21], a pressure induced enhancement of its superconducting transition temperature is in coincidence with the appearance of pressure induced CDW-type features of the temperature dependent electrical resistivity [22].

In the present work we investigate two lutetium 3*d*-metal dicarbides, $LuNiC_2$ and $LuCoC_2$ as well as the series $Lu(Ni_{1-x}Co_x)C_2$ with respect to their solid solubility, crystal structure and the evolution of CDW order. $LuNiC_2$ was earlier reported to display a quasi-one-dimensional electronic structure and the highest, among $RNiC_2$, CDW transition temperature $T_{CDW} \cong$ 450 K, while $LuCoC_2$ displays an essentially three-dimensional electronic structure and no CDW order [8]. As the evolution of CDW order revealed to be barely traceable for polycrystalline solid solutions $Lu(Ni_{1-x}Co_x)C_2$ prepared by standard arc-melting techniques, we finally employed the floating-zone melting technique for preparing samples with improved homogeneity with respect to their Ni/Co stoichiometry. We investigated the gradual suppression of CDW order with increasing levels of non-isoelectronic substitution of Ni by Co and, finally, determined a critical composition for the suppression of CDW order.

2. Experimental procedures

2.1. Alloy preparation

Polycrystalline samples of composition $Lu(Ni_{1-x}Co_x)C_2$ (x = 0, 0.025, 0.05, 0.075, 0.1, 0.2, 0.3, 0.4, 0.5, 0.66, 0.75, 0.8, 1.0) were prepared from commercially available elements: Lu sublimed bulk pieces, 99.99 wt% (Alfa Aesar, Johnson Matthey Company), powders of electrolytic nickel and cobalt (Strem Chemicals, purity of 99.99 wt%) and graphite powder, 99.98 wt% (Aldrich). Lutetium metal was filed to coarse powders with beryllium bronze files (Dönges GmbH, Germany). Mixtures of the components were compacted in stainless steel dies. The pellets of ~1 g were arc-melted under purified argon atmosphere on a water-cooled copper hearth, turned over and re-melted typically three times to improve homogeneity. The samples were then wrapped in tantalum foil enclosed in an evacuated silica ampule, annealed at 1070 K for one month, and then quenched in cold water.

2.2. Crystal growth and energy-dispersive x-ray spectroscopy

Pseudo ternary solid solutions $Lu(Ni_{1-x}Co_x)C_2$ with x = 0.08, 0.14, 0.16. 0.2 were grown from polycrystalline feed rods via the floating zone technique in an optical mirror furnace (Crystal Systems Corporation, Japan) and partially single crystalline samples with variable sizes of crystal domains were obtained. We note, that the floating zone melting process of these pseudo-ternary compositions is markedly less stable than that of ternary $RNiC_2$ and, for some of them, necessitated repeated attempts to grow reasonably sized samples. Grown ingots were initially checked via polarization contrast optical microscopy and a single crystalline sample $LuNi_{0.92}Co_{0.08}C_2$ was oriented by means of the Laue method. For other pseudo-ternary samples, crystalline domains were too small to facilitate the preparation of sizeable, oriented single crystalline samples, which were thus cut and measured as randomly oriented multicrystalline samples (with single crystalline domains up to mm-size and spot-wise reasonable Laue patterns). $LuNiC_2$ and $LuCoC_2$ single crystals used also for the current DTA measurements were grown previously according to procedures described in Ref. [8].

A cross section of $LuNi_{0.92}Co_{0.08}C_2$ grown via floating zone melting was examined along the growth direction with scanning electron microscopy (SEM) using a Philips XL30 ESEM with EDAX XL-30 EDX detector. These data revealed an initial deviation of the crystal stoichiometry towards $LuNi_{0.9}Co_{0.1}C_2$, which is in line with the higher melting point of $LuCoC_2$ as compared to $LuNiC_2$. With progressing growth of just a few millimeters, the stoichiometry approached to the nominal stoichiometry of the polycrystalline feed rod.

2.3. Powder x-ray diffraction

Powder X-ray diffraction (PXRD) studies were conducted with an *Aeris* powder diffractometer by Malvern Panalytica with Cu K_α radiation ($10^\circ \leq 2\theta \leq 120^\circ$, step size 0.01°). Precise lattice parameters and standard deviations were derived by least-square refinement of room temperature PXRD data using the WinCSD software package [23]. LaB_6 (NIST Standard Reference Material 660b, a = 4.15689 Å) served as internal standard. In order to check the homogeneity of the samples Rietveld profile refinements of the X-ray powder pattern were performed using FullProf and WinCSD software [23,24].

2.4. Differential thermal analysis

Melting points of crystal pieces of $LuNiC_2$, $LuCoC_2$ (preparation reported in Ref. [8]) and pseudo-ternary samples $LuNi_{0.8}Co_{0.2}C_2$, $LuNi_{0.5}Co_{0.5}C_2$, and $LuNi_{0.2}Co_{0.8}C_2$ were studied by means of differential thermal analysis (DTA) with a commercial *Linseis DTA PT 1750*. DTA measurements were performed in a flowing atmosphere of high purity Ar (99.999%). For each sample, two pieces with a total mass of about 200 mg were placed in an alumina crucible. The calibration was conducted with high purity Ag (99,9999%, T_m = 1234.9 K) and Ni (99,99%, T_m = 1728 K). The samples were studied in the range from room temperature to 2000 K at a heating and cooling rate of 10 K/min. The error was estimated by measuring the melting point of Ni. The thermal effects of phase transitions obtained from the DTA curves were evaluated with an approximate accuracy ± 10 K.

2.5. Physical properties

The temperature dependent electrical resistivity of bar shape $Lu(Ni_{1-x}Co_x)C_2$ samples was measured with a four-probe technique in a Quantum Design, Physical Properties Measurement System (PPMS) system at a temperature interval 2–400 K. With use of a PPMS ^{3}He-insert, two samples grown via the floating zone technique, i.e. $LuNi_{0.84}Co_{0.16}C_2$ and $LuNi_{0.8}Co_{0.2}C_2$, were additionally measured down to 0.4 K. Thin gold wires were fixed to the samples via spark welding, thus, serving as solid electrical contacts for resistivity studies. Heat capacity data of typically 50 mg samples prepared via floating zone melting were collected with a Quantum Design PPMS using a relaxation-type method in the temperature range from 2 to 320 K and heat capacity data of typically 1 g polycrystalline samples with a home-made calorimeter employing an adiabatic step-heating technique in the temperature interval 2–80 K. In both cases, Apiezon-N grease was used as a thermal contact medium.

3. Results and discussion

3.1. Structural characterization

Fig. 1 shows the XRD profiles of powdered $LuNiC_2$, $LuCoC_2$ and

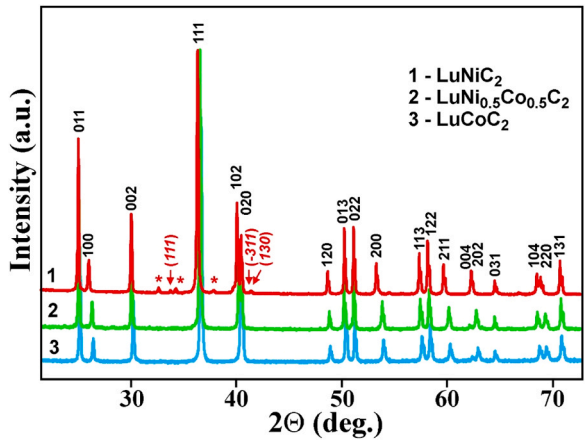

Fig. 1. XRD profiles of powdered specimens of $LuNiC_2$, $Lu(Ni_{0.5}Co_{0.5})C_2$, and $LuCoC_2$ with indexed reflections according to the space group *Amm*2 (structure type $CeNiC_2$); (*) marks reflections assigned to the impurity phase $Lu_4Ni_{13}C_4$ [25] and (↓, hkl) points on reflections related to the CDW superstructure modulation of $LuNiC_2$ [8].

$LuNi_{0.5}Co_{0.5}C_2$. XRD data of the $Lu(Ni_{1-x}Co_x)C_2$ series were indexed in the $CeNiC_2$ structure type, space group *Amm*2, thus, confirming a continuous solid solubility between $LuNiC_2$ and $LuCoC_2$. The present results of $LuNiC_2$ and $LuCoC_2$ are in good agreement with earlier reported data in Refs. [1,8].

To prove the crystal structure model, a full profile refinement has been performed on the sample with composition $LuNi_{0.8}Co_{0.2}C_2$. The PXRD profiles (experimental and calculated) are shown in Fig. 2. The $CeNiC_2$ structure-type arrangement for $LuNi_{0.8}Co_{0.2}C_2$ with one position being statistically occupied by a mixture $M = 0.8Ni + 0.2Co$ is confirmed as arising from the small values of the reliability factors ($R_{B(I)} = 3.4\%$, $R_p = 2.2\%$). The unit cell of the $Lu(Ni_{1-x}Co_x)C_2$ series is presented as inset of Fig. 2. Along crystallographic direction [100], the structure reveals two different layers forming by lutetium atoms (one layer, yellow planes in the inset of Fig. 2) and *M* atoms together with C-C dumbbells (another layer, blue plane in the inset of Fig. 2). The refined atomic coordinates, displacement parameters, and interatomic distances for $LuNi_{0.8}Co_{0.2}C_2$ are summarized in Table 1. According to *Amm*2 space group, the 2*a* site has coordinates (0, 0, *z*), thus, to preserve reasonable interatomic distances, coordinates were fixed at $z = 0$ for Lu atoms.

The unit cell parameters as refined for 15 samples of the $Lu(Ni_{1-x}Co_x)C_2$ ($0 \le x \le 1$) series are gathered in Table 2. The positions of PXRD reflections of all the investigated compositions have been refined with the peak positions of the internal standard LaB_6 as a reference. The change of unit cell parameters across the $Lu(Ni_{1-x}Co_x)C_2$ solid solutions series follows a non-linear behavior upon *x*, as shown in Fig. 3.

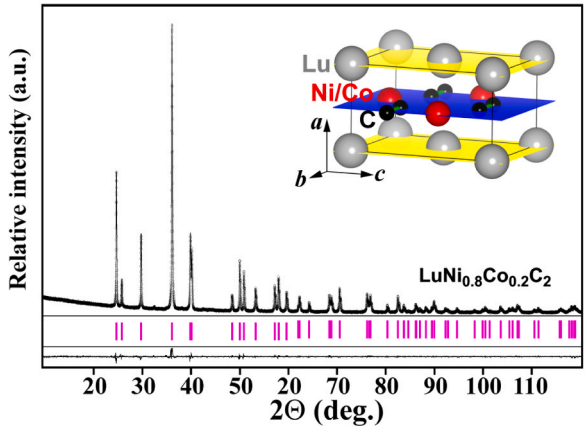

Fig. 2. Experimental and refined PXRD patterns of the $LuNi_{0.8}Co_{0.2}C_2$ sample (Cu K_α radiation) together with the atomic arrangement within a unit cell (the two-layered structure along [100], as indicated).

Table 1
Atomic coordinates and selected interatomic distances in the crystal structure of the continuous solid solution $Lu(Ni_{1-x}Co_x)C_2$, at $x = 0.2$ ($M = 0.8Ni + 0.2Co$, fixed).

Atom	Site	*x*	*y*	*z*	B_{iso}, Å^2
Lu	2*a*	0	0	0*	0.48(1)
M	2*b*	½	0	0.6145(5)	0.90(2)
C	4*e*	½	0.154(3)	0.302(3)	0.69(3)
$d_{Lu\text{-}Lu}$, Å	3.4391(2)	3.7413(1)	$d_{M\text{-}C}$, Å	1.912(15)	2.00(2)
$d_{Lu\text{-}M}$, Å	2.879(2)	2.908(1)	$d_{C\text{-}C}$, Å	1.38(2)	
$d_{Lu\text{-}C}$, Å	2.585(3)	2.602(3)			

* fixed coordinate

Table 2
The unit cell parameters as function of the Ni/Co composition of pseudo-ternary solid solutions $Lu(Ni_{1-x}Co_x)C_2$.

Composition *x*	*a* (Å)	*b* (Å)	*c* (Å)	*V* (Å^3)
0.0	3.4500(2)	4.4786(2)	5.9859(2)	92.49
0.025	3.44929(5)	4.48035(8)	5.98521(9)	92.50
0.05	3.44807(9)	4.4826(2)	5.9852(2)	92.51
0.075	3.44646(8)	4.4838(1)	5.9848(1)	92.49
0.1	3.4452(2)	4.4842(2)	5.9850(1)	92.46
0.14	3.44414(7)	4.48512(8)	5.98527(8)	92.46
0.16	3.44156(6)	4.4857(1)	5.9877(1)	92.44
0.2	3.4391(2)	4.4859(1)	5.9888(2)	92.39
0.3	3.4332(1)	4.4866(1)	5.9926(2)	92.31
0.4	3.4337(1)	4.4861(2)	5.9930(1)	92.30
0.5	3.4238(2)	4.4858(2)	6.0009(2)	92.16
0.66	3.41898(7)	4.48594(9)	6.00501(9)	92.10
0.75	3.41772(5)	4.48670(7)	6.00278(6)	92.05
0.8	3.41796(7)	4.4868(1)	6.00078(10)	92.03
1.0	3.42079(8)	4.4882(1)	5.9888(1)	91.95

The unit cell volume decreases with increasing Co content with a non-linear deviation from Vegard's rule, as it was observed for the related series $Dy(Ni_{1-x}Co_x)C_2$ and $Ho(Ni_{1-x}Co_x)C_2$ [15,16]. A local demotion of the *a* cell parameter and elevation of the *c* cell parameter is observed from $LuNiC_2$ up to $LuNi_{0.33}Co_{0.67}C_2$ keeping the almost monotonous decrease of the unit cell volume of the series $Lu(Ni_{1-x}Co_x)C_2$. The lattice parameter *a* defines the nearest Lu–Lu and *M*–*M* {$M = (1 - x)Ni + xCo$} distances (see Fig. 2, Table 1) which change corresponding to the descending of the lattice volume. The non-linear variation of the *a* and *c* lattice parameters is attributed to the effect of non-isoelectronic substitution of Ni by Co where one extra electron is progressively subtracted in the series $Lu(Ni_{1-x}Co_x)C_2$.

3.2. DTA analysis

Fig. 4 shows the high-temperature parts of DTA heating curves measured for solid solutions $Lu(Ni_{1-x}Co_x)C_2$. Within the studied temperature range from room temperature to 2000 K there was only one signal on each DTA heating and cooling curves indicating a congruent melting of the compounds. The system $LuNiC_2$–$LuCoC_2$ is, thus, a pseudo-binary one. The melting points are defined as the onset of the endothermic peaks in the warming segment of DTA profiles. Our data reveal an increase of the melting temperatures with increasing content of Co in this series. No changes in the samples after DTA measurements were detected by PXRD method. According to the DTA data, a $LuNiC_2$–$LuCoC_2$ pseudo-binary phase diagram has been constructed and it is shown in Fig. 5. The only two-phase equilibrium between liquid (*L*) and solid (δ) solutions occurs in the system. Curvatures of liquidus and solidus curves change within comparatively narrow temperature range of 1874 – 1970 ± 10 K. Upraise of temperatures of liquidus and solidus curves is the highest in the composition range $0 \le x < 0.2$, while for

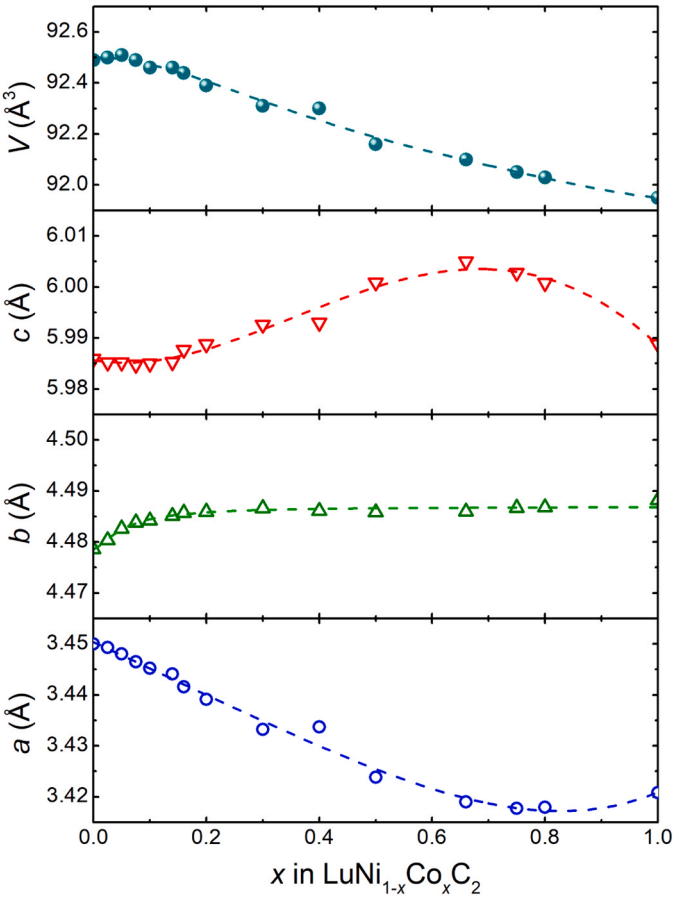

Fig. 3. Composition dependent variation of the lattice parameters and unit cell volumes of continuous solid solutions $Lu(Ni_{1-x}Co_x)C_2$. Dashed lines are guides to the eye.

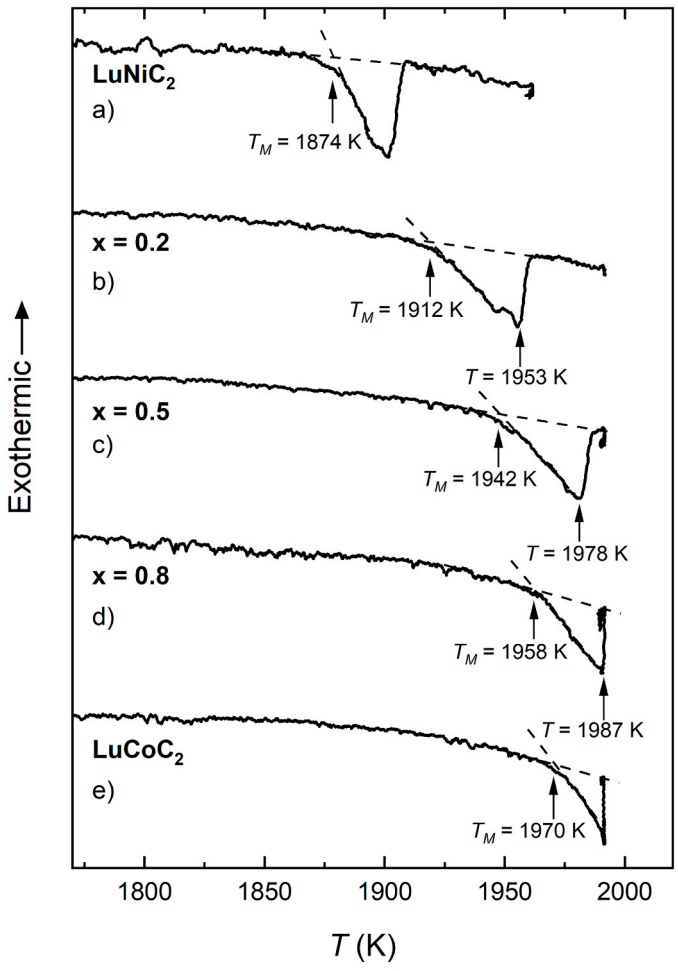

Fig. 4. DTA heating curves measured for samples *a*) $LuNiC_2$, *b*) $LuNi_{0.8}Co_{0.2}C_2$, *c*) $LuNi_{0.5}Co_{0.5}C_2$, *d*) $LuNi_{0.2}Co_{0.8}C_2$, and *e*) $LuCoC_2$. Phase transformation temperatures are indicated.

compositions with higher Co content $x > 0.2$ the line profiles are smoother. Such peculiarities of the phase diagram may explain problems for obtaining single crystals of good quality and homogeneity for the compositions of the solid solutions with $x > 0.2$.

3.3. Electrical resistivity

A search for the evolution of CDW order in solid solutions $Lu(Ni_{1-x}Co_x)C_2$ is motivated by our earlier studies which demonstrated for $LuNiC_2$ a commensurate CDW order below 447(5) K, while for $LuCoC_2$ there is no indication of a CDW transition nor any other structural transition down to low temperatures [8]. Our investigation of the temperature dependent electrical resistivity of polycrystalline solid solutions $Lu(Ni_{1-x}Co_x)C_2$ revealed visible CDW features only in a very narrow range of Ni-rich solid solutions. The corresponding temperature dependent resistivity data of polycrystalline $Lu(Ni_{1-x}Co_x)C_2$ with $x = 0.025$, 0.05, and 0.075 are displayed in Fig. 6 together with data of polycrystalline $LuNiC_2$ reported earlier in Ref. [8]. These results reveal an evolution of CDW features: increasing levels of the substitution of Ni by Co causes a systematic reduction of the CDW transition temperature which is accompanied with a rapid broadening of the CDW anomaly of the electrical resistivity such that it becomes essentially untraceable for compositions $x = 0.1$ or higher. The rapid broadening of the transition is attributed to inhomogeneity of the polycrystalline solid solutions with respect to their Ni/Co stoichiometry.

For obtaining samples with improved homogeneity with respect to their Ni/Co stoichiometry, additional solid solutions were prepared with the floating zone melting technique, which in the case of $LuNi_{0.92}Co_{0.08}C_2$, allowed to prepare a bar-shape single crystalline sample for

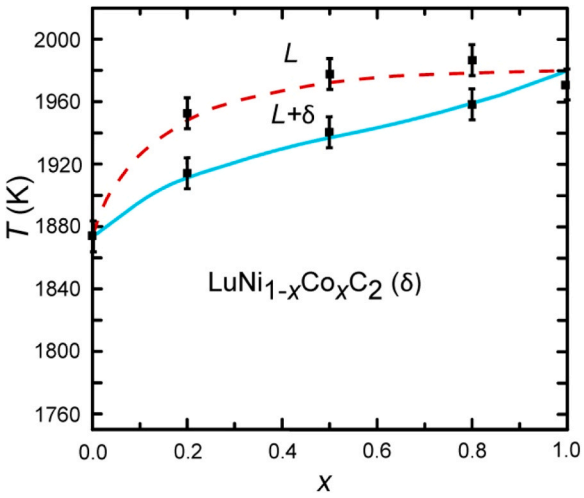

Fig. 5. $LuNiC_2$–$LuCoC_2$ pseudo-binary phase diagram. Dashed and solid lines are guides to the eye.

electrical resistivity measurements. Other multi-crystalline pseudo-ternary samples obtained from floating zone melting were cut with random orientations. Due to the significant anisotropy of the electrical resistivity of $RNiC_2$ compounds [6,8,26], absolute values of the

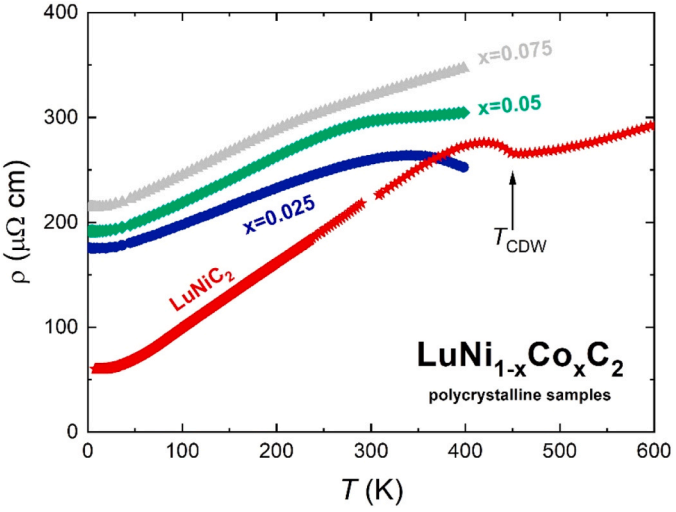

Fig. 6. Temperature dependent electrical resistivity of Ni-rich polycrystalline solid solutions $Lu(Ni_{1-x}Co_x)C_2$. Data of polycrystalline $LuNiC_2$, as reported in Ref. [8], are included for direct comparison. Red: $x = 0$, dark blue: $x = 0.025$, turquoise: $x = 0.05$, grey $x = 0.075$.

electrical resistivity of floating zone grown solid solutions, when using different batches of the same composition or different bars cut from the same sample, are reproducible within a factor of the order of two. Accordingly, and for better visibility and comparability of relevant features (the sake of clarity) we adjusted the resistivity data of our floating zone grown solid solutions, which are presented in Fig. 7, by factors ranging between 0.7 and 1.5. Single crystalline $LuNi_{0.92}Co_{0.08}C_2$ was measured with current parallel to the orthorhombic *a*-axis (i.e., $I \,||\, [100]$) and, for comparison with the ternary parent phase, we include earlier reported $LuNiC_2$ single crystal data measured with the same orientation, $I \,||\, a$ [8]. These data, when being analyzed for the strongest change in slope, reveal a systematic reduction of the CDW transition temperature from 447(5) K for $LuNiC_2$ to 310(10) K for $LuNi_{0.92}Co_{0.08}C_2$ and finally to 140(15) K for $LuNi_{0.86}Co_{0.14}C_2$, while the resistivity curves of $LuNi_{0.84}Co_{0.16}C_2$ and $LuNi_{0.8}Co_{0.2}C_2$ remain equally featureless with no sufficiently obvious trace of a CDW transition. A critical composition for the suppression of CDW order in solid solutions $Lu(Ni_{1-x}Co_x)C_2$ is, thus, expected near $x = 0.15 - 0.17$.

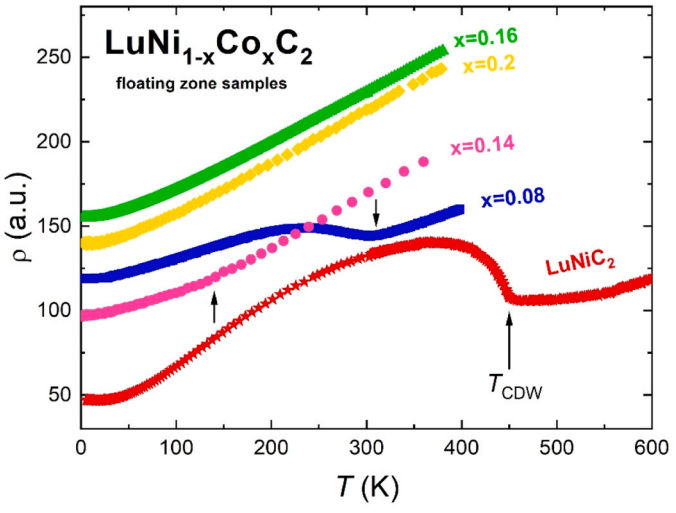

Fig. 7. Temperature dependent electrical resistivity of Ni-rich solid solutions $Lu(Ni_{1-x}Co_x)C_2$ prepared via the floating zone melting technique. Data of single crystalline $LuNiC_2$, as reported in Ref. [8], are included for a direct comparison. Red: $x = 0$ ($I \,||\, [100]$), dark blue: $x = 0.08$ ($I \,||\, [100]$), pink: $x = 0.14$, green $x = 0.16$, yellow: $x = 0.2$.

3.4. Heat capacity

The resistivity studies have been complemented by heat capacity measurement of selected solid solutions, which however, could not resolve anomalies related to the CDW transitions indicated by the electrical resistivity data of $LuNi_{0.92}Co_{0.08}C_2$ and $LuNi_{0.86}Co_{0.14}C_2$. We, thus, focus our analysis of the heat capacity data of solid solutions $Lu(Ni_{1-x}Co_x)C_2$ on their *T*-linear electronic contributions. From the low temperature heat capacity data in Fig. 8, displayed as c_p/T vs. T^2, we extract the electronic Sommerfeld coefficient γ (via the commonly applied linear extrapolation of the data to $T = 0$ K), which provides a measure for the electronic density of states at the Fermi energy. The DFT calculated electronic density of states at the Fermi level, $N(E_F)$, of the orthorhombic $CeNiC_2$-type high-temperature structure of $LuNiC_2$ was reported as $N(E_F) \approx 1.03$ states/eV per f.u. and implies a bare electronic Sommerfeld coefficient $\gamma \approx 2.43$ mJ/mol-K^2 which markedly exceeds the experimental Sommerfeld coefficient $\gamma = 0.83(5)$ mJ/mol-K^2 [8]. The significantly reduced value of γ results from a significant reduction of the electronic density of states $N(E_F)$ due CDW order and corresponding CDW gap formation [8]. It is thus remarkable that the Sommerfeld γ-values obtained for solid solutions with $x = 0.14 - 0.5$, i.e. $\gamma \approx 2.4 - 2.6$ mJ/mol-K^2, are all close to the value expected for the orthorhombic parent-structure of $LuNiC_2$, i.e., without CDW modulation. We, thus, summarize in Fig. 9 the evolution of the electronic Sommerfeld coefficients of solid solutions $Lu(Ni_{1-x}Co_x)C_2$ and compare it with the evolution of CDW anomalies of the electrical resistivity shown in Fig. 7. The onset of the significant drop of the composition dependent Sommerfeld coefficient $\gamma(x)$ which is seen for Ni-rich solid solution, i.e., for $Lu(Ni_{1-x}Co_x)C_2$ with $x \leq 0.14$, closely coincides with critical composition of CDW order as indicated by the electrical resistivity data. The CDW ordering temperatures evaluated from electrical resistivity curves and the electronic Sommerfeld coefficients estimated from the low temperature heat capacity as a function of the Co content *x* of $Lu(Ni_{1-x}Co_x)C_2$ are summarized in Table 3.

In order to check for a possible appearance of a superconducting dome in the vicinity of the critical composition of CDW order, we investigated the low temperature electrical resistivity of two samples, $LuNi_{0.84}Co_{0.16}C_2$ and $LuNi_{0.8}Co_{0.2}C_2$, which are closest to the critical composition for the suppression of CDW order, with a ^{3}He cryo-system. These experiments did not reveal any evidence of superconductivity

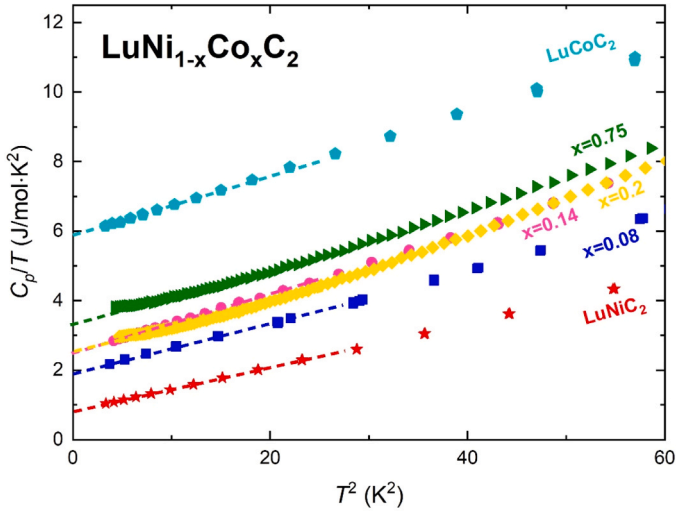

Fig. 8. Low temperature heat capacity data of selected solid solutions $Lu(Ni_{1-x}Co_x)C_2$ in a c_p/T vs. T^2 representation. Single crystal data of $LuNiC_2$ and $LuCoC_2$ [8] are included for a direct comparison. Red: $x = 0$, dark blue: $x = 0.08$, pink: $x = 0.14$, yellow: $x = 0.2$, dark green $x = 0.75$, turquoise $x = 1$.

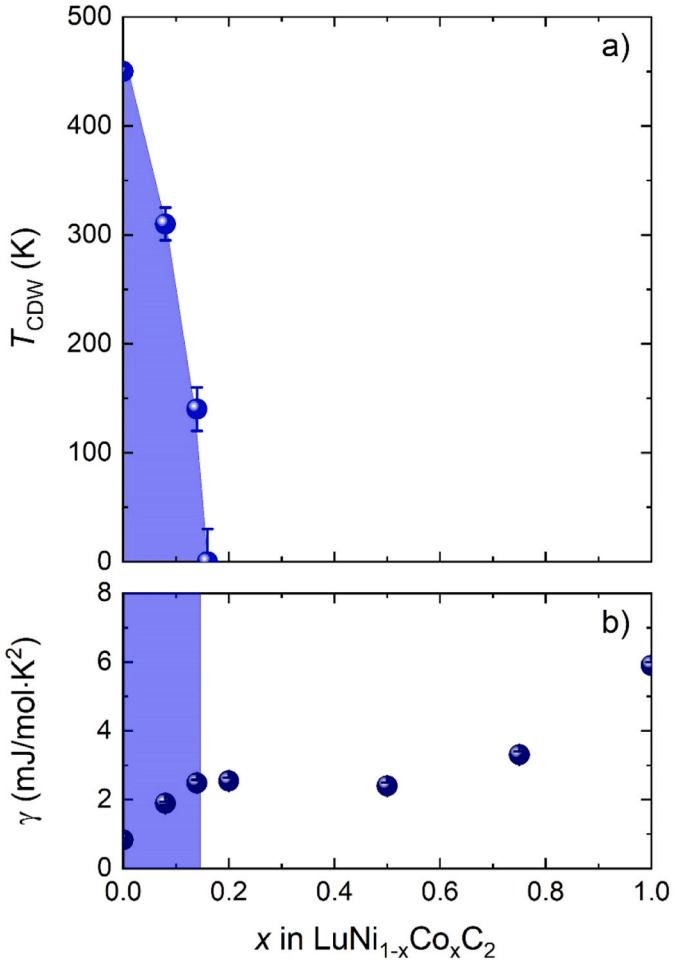

Fig. 9. Evolution of CDW anomalies as observed from electrical resistivity studies (a) and Sommerfeld coefficients (b) as function of the Ni/Co composition of $Lu(Ni_{1-x}Co_x)C_2$.

Table 3
Composition-dependent CDW ordering temperatures and electronic Sommerfeld coefficients of solid solutions $Lu(Ni_{1-x}Co_x)C_2$. Values for $x = 0$ and 1 are taken from Ref. [8].

composition x	T_{CDW} (K)	γ (mJ/mol-K^2)
0.0	447 (5)	0.83(5)
0.08	310 (10)	1.89(8)
0.14	140 (15)	2.48(10)
0.2	-	2.54 (10)
0.5	-	2.4 (1)
0.75	-	3.3 (1)
1.0	-	5.9 (1)

down to 0.38 K. The fact that superconductivity is pressure-enhanced in $LaNiC_2$ [22], presumably by fluctuation of the CDW order parameter, while it appears absent near the critical point of CDW in the system $Lu(Ni_{1-x}Co_x)C_2$, may relate to the different nature of CDW phases in $RNiC_2$ with light and heavy lanthanides. CDW order of the former reduces only translation symmetries [27], whereas CDW order in latter reduces translation and point group symmetry [8] and, as demonstrated by comparing various experimental features of the corresponding CDW states, distinctly different CDW symmetry changes appear to cause rather different changes of the electronic structure in the CDW ordered states [26].

4. Conclusions

Substitution of Ni by Co in the ternary compound $LuNiC_2$ ($CeNiC_2$-type structure, space group *Amm*2) results in a continuous solid solution $Lu(Ni_{1-x}Co_x)C_2$. The unit cell parameters decrease with increasing Co content with a non-linear deviation from Vegard's rule within the solid solution which is associated with non-isoelectronic Ni/Co substitution. DTA heating and cooling curves indicate congruent melting of ternary compounds and reveal an increase of the melting temperatures with increasing content of Co in this series of alloys. Based on DTA data, a phase diagram of the pseudo-binary $LuNiC_2$–$LuCoC_2$ system was constructed showing a single two-phase equilibrium between liquid and solid solutions. Temperature ranges of continuous liquid and solid solutions $Lu(Ni_{1-x}Co_x)C_2$ were evaluated. Our physical properties measurements, both on poly- and single-crystalline $Lu(Ni_{1-x}Co_x)C_2$ samples, show that CDW order, which occurs at $T_{CDW} \cong 450$ K in $LuNiC_2$, is consistently suppressed with increasing Co content x of these solid solutions and finally, for $x > 0.15$, features of CDW ordering are no longer observed. The suppression of CDW order is further corroborated by the evolution of the electronic Sommerfeld coefficient, which significantly decreases for $x < 0.15$ and thus reflects the CDW gap formation in Ni-richest solid solutions. A critical composition for the suppression of CDW order in the series $Lu(Ni_{1-x}Co_x)C_2$ is expected in near $x \approx 0.15$–0.17 where no evidence of emerging superconductivity has been revealed down to 0.38 K.

CRediT authorship contribution statement

All authors contributed equally.

Declaration of Competing Interest

The authors declare that they have no known competing financial interests or personal relationships that could have appeared to influence the work reported in this paper.

Data availability

Data will be made available on request.

Acknowledgements

Financial support for M.R. by grant BPN/BEK/2021/1/00245/DEC/1 of The Polish National Agency for Academic Exchange (NAWA) is gratefully acknowledged. **V.L. thanks DFG (Deutsche Forschungsgemeinschaft) for financial support (project No. 467257848)**. Metallography support by Snezana Stojanovic and support with SEM microprobe analysis by Monika Waas and Robert Svagera is gratefully acknowledged. The authors acknowledge TU Wien Bibliothek for financial support through its Open Access Funding Programme.

References

[1] W. Jeitschko, M. Gerss, Ternary carbides of the rare earth and iron group metals with $CeCoC_2$- and $CeNiC_2$-type structure, J. Less Common Met. 116 (1986) 147–157, https://doi.org/10.1016/0022-5088(86)90225-0.
[2] O.I. Bodak, E.P. Marusin, V.A. Bruskov, Crystal structure of compounds $RCoC_2$ (R = Ce, La, or Pr), Sov. Phys. Crystallogr. 25 (1980) 355-356 [Transl. Krist. 25 (1980) 617–619 (in Russian)].
[3] V. Babizhetskyy, B. Kotur, V. Levytskyy, H. Michor, Alloy systems and compounds containing rare earth metals and carbon. Handb. Phys. Chem. Rare Earths. 52, North-Holl., Amst., 2017, pp. 1–263, https://doi.org/10.1016/bs.hpcre.2017.09.001.
[4] M. Murase, A. Tobo, H. Onodera, Y. Hirano, T. Hosaka, S. Shimomura, N. Wakabayashi, Lattice constants, electrical resistivity and specific heat of $RNiC_2$, J. Phys. Soc. Jpn. 73 (2004) 2790–2794, https://doi.org/10.1143/JPSJ.73.2790.
[5] S. Shimomura, C. Hayashi, G. Asaka, N. Wakabayashi, M. Mizumaki, H. Onodera, Charge-density-wave destruction and ferromagnetic order in $SmNiC_2$, Phys. Rev. Lett. 102 (2009) 076404, https://doi.org/10.1103/PhysRevLett.102.076404.

[6] S. Shimomura, C. Hayashi, N. Hanasaki, K. Ohnuma, Y. Kobayashi, H. Nakao, M. Mizumaki, H. Onodera, Multiple charge density wave transitions in the antiferromagnets RNiC$_2$ (R = Gd, Tb), Phys. Rev. B 93 (2016) 165108, https://doi.org/10.1103/PhysRevB.93.165108.
[7] M. Roman, J. Strychalska-Nowak, T. Klimczuk, K.K. Kolincio, Extended phase diagram of RNiC$_2$ family: Linear scaling of the Peierls temperature (R), Phys. Rev. B 97 (2018) 041103, https://doi.org/10.1103/PhysRevB.97.041103.
[8] S. Steiner, H. Michor, O. Sologub, B. Hinterleitner, F. Höfenstock, M. Waas, E. Bauer, B. Stöger, V. Babizhetskyy, V. Levytskyy, B. Kotur, Single crystal study of the charge density wave metal LuNiC$_2$, Phys. Rev. B 97 (2018) 205115, https://doi.org/10.1103/PhysRevB.97.205115.
[9] H. Maeda, R. Kondo, Y. Nogami, Multiple charge density waves compete in ternary rare-earth nickel carbides, RNiC$_2$ (R: Y, Dy, Ho, and Er), Phys. Rev. B 100 (2019) 104107, https://doi.org/10.1103/PhysRevB.100.104107.
[10 K.K. Kolincio, M. Roman, T. Klimczuk, Charge density wave and large nonsaturating magnetoresistance in YNiC$_2$ and LuNiC$_2$, Phys. Rev. B 99 (2019) 205127, https://doi.org/10.1103/PhysRevB.99.205127.
[11] V. Levytskyi, P. Wyzgab, O. Isnard, V. Babizhetskyy, B. Kotur, Heat capacity and high temperature electrical transport properties of TbNiC$_2$, Solid State Sci 108 (2020) 106396, https://doi.org/10.1016/j.solidstatesciences.2020.106396.
[12] H. Michor, A. Schumer, M. Hembara, B. Kotur, V. Levytskyy, V. Babizhetskyy, The quasi-binary system CeCoC$_2$–CeNiC$_2$: crystal structure and physical properties, Solid State Phenom. 289 (2019) 114–119, https://doi.org/10.4028/www.scientific.net/SSP.289.114.
[13] W. Kockelmann, W. Schäfer, J.K. Yakinthos, P.A. Kotsanidis, Crossover from ferromagnetic RCoC$_2$ to antiferromagnetic RNiC$_2$ (R = rare earths) investigated on mixed Tb(Co,Ni)C$_2$, J. Magn. Magn. Mater. 177-181 (1998) 792–794, https://doi.org/10.1016/S0304-8853(97)00725-7.
[14] V. Levytskyy, V. Babizhetskyy, O. Myakush, J.-F. Halet, B. Kotur, Ternary carbides of the rare earth and 3-d metals containing C$_2$ units: the crystal structure of Dy(Co$_{1-x}$Ni$_x$)C$_2$, Visnyk Lviv Univ. Ser. Chem. 53 (2012) 97–102.
[15] H. Michor, V. Levytskyy, F. Schwarzböck, V. Babizhetskyy, B. Kotur, Evolution of magnetic properties in the solid solution DyCo$_{1-x}$Ni$_x$C$_2$, J. Magn. Magn. Mater. 374 (2015) 553–558, https://doi.org/10.1016/j.jmmm.2014.08.085.
[16] H. Michor, S. Steiner, A. Schumer, M. Hembara, V. Levytskyy, V. Babizhetskyy, B. Kotur, Magnetic properties of HoCoC$_2$, HoNiC$_2$ and their solid solutions, J. Magn. Magn. Mater. 441 (2017) 69–75, https://doi.org/10.1016/j.jmmm.2017.05.038.
[17] T. Gruner, D. Jang, Z. Huesges, R. Cardoso-Gil, G.H. Fecher, M.M. Koza, O. Stockert, A.P. Mackenzie, M. Brando, C. Geibel, Charge density wave quantum critical point with strong enhancement of superconductivity, Nat. Phys. 13 (2017) 967–972, https://doi.org/10.1038/nphys4191.
[18] W.H. Lee, H.K. Zeng, Y.D. Yao, Y.Y. Chen, Superconductivity in the Ni based ternary carbide LaNiC$_2$, Phys. C: Supercond. Appl. 266 (1996) 138–142, https://doi.org/10.1016/0921-4534(96)00309-7.
[19] V.K. Pecharsky, L.L. Miller, K.A. Gschneidner Jr, Low-temperature behavior of two ternary lanthanide nickel carbides: superconducting LaNiC$_2$ and magnetic CeNiC$_2$, Phys. Rev. B 58 (1998) 497–502, https://doi.org/10.1103/PhysRevB.58.497.
[20] A.D. Hillier, J. Quintanilla, R. Cywinski, Evidence for Time-Reversal Symmetry Breaking in the Noncentrosymmetric Superconductor LaNiC$_2$, Phys. Rev. Lett. 105 (2009) 229901, https://doi.org/10.1103/PhysRevLett.102.117007.
[21] S. Sundar, S.R. Dunsiger, S. Gheidi, K.S. Akella, A.M. Côté, H.U. Özdemir, N.R. Lee-Hone, D.M. Broun, E. Mun, F. Honda, Y.J. Sato, T. Koizumi, R. Settai, Y. Hirose, I. Bonalde, J.E. Sonier, Two-gap time reversal symmetry breaking superconductivity in noncentrosymmetric LaNiC$_2$, Phys. Rev. B 103 (2021) 014511, https://doi.org/10.1103/PhysRevB.103.014511.
[22] S. Katano, H. Nakagawa, K. Matsubayashi, Y. Uwatoko, H. Soeda, T. Tomita, H. Takahashi, Anomalous pressure dependence of the superconductivity in noncentrosymmetric LaNiC$_2$: evidence of strong electronic correlations (R), Phys. Rev. B 90 (2014) 220508, https://doi.org/10.1103/PhysRevB.90.220508.
[23] L. Akselrud, Y. Grin, WinCSD: software package for crystallographic calculations (Version 4), J. Appl. Crystallogr. 47 (2014) 803–805, https://doi.org/10.1107/S1600576714001058.
[24] J. Rodriguez-Carvajal, Recent developments of the program FULLPROF. Commission on powder diffraction (IUCr), Newsl 26 (2001) 12–19.
[25] A.A. Putyatin, Systems Er(Tm, Yb, Lu)–Ni–C and crystallization of diamonds under pressures above 5.7 GPa, Inorg. Mater. 27 (1991) 1299–1301.
[26] M. Roman, M. Fritthum, B. Stöger, D.T. Adroja, H. Michor, Charge density wave and crystalline electric field effects in TmNiC$_2$, Phys. Rev. B 107 (2023) 125137, https://doi.org/10.1103/PhysRevB.107.125137.
[27] A. Wölfel, L. Li, S. Shimomura, H. Onodera, S. van Smaalen, Commensurate charge-density wave with frustrated interchain coupling in SmNiC$_2$, Phys. Rev. B 82 (2010) 054120, https://doi.org/10.1103/PhysRevB.82.054120.